doi:10.1093/brain/awx003 BRAIN 2017: 140; 1107–1116 | 1107

BRAIN
A JOURNAL OF NEUROLOGY

MRI-visible perivascular space location is associated with Alzheimer's disease independently of amyloid burden

Gargi Banerjee,[1] Hee Jin Kim,[2,3] Zoe Fox,[4] H. Rolf Jäger,[5] Duncan Wilson,[1] Andreas Charidimou,[1] Han Kyu Na,[2] Duk L. Na,[2,3] Sang Won Seo[2,3] and David J. Werring[1]

Perivascular spaces that are visible on magnetic resonance imaging (MRI) are a neuroimaging marker of cerebral small vessel disease. Their location may relate to the type of underlying small vessel pathology: those in the white matter centrum semi-ovale have been associated with cerebral amyloid angiopathy, while those in the basal ganglia have been associated with deep perforating artery arteriolosclerosis. As cerebral amyloid angiopathy is an almost invariable pathological finding in Alzheimer's disease, we hypothesized that MRI-visible perivascular spaces in the centrum semi-ovale would be associated with a clinical diagnosis of Alzheimer's disease, whereas those in the basal ganglia would be associated with subcortical vascular cognitive impairment. We also hypothesized that MRI-visible perivascular spaces in the centrum semi-ovale would be associated with brain amyloid burden, as detected by amyloid positron emission tomography using ^{11}C-Pittsburgh B compound (PiB-PET). Two hundred and twenty-six patients (Alzheimer's disease $n = 110$; subcortical vascular cognitive impairment $n = 116$) with standardized MRI and PiB-PET imaging were included. MRI-visible perivascular spaces were rated using a validated 4-point visual rating scale, and then categorized by severity ('none/mild', 'moderate' or 'frequent/severe'). Univariable and multivariable regression analyses were performed. Those with Alzheimer's disease-related cognitive impairment were younger, more likely to have a positive PiB-PET scan and carry at least one apolipoprotein E $\varepsilon 4$ allele; those with subcortical vascular cognitive impairment were more likely to have hypertension, diabetes mellitus, hyperlipidaemia, prior stroke, lacunes, deep microbleeds, and carry the apolipoprotein E $\varepsilon 3$ allele. In adjusted analyses, the severity of MRI-visible perivascular spaces in the centrum semi-ovale was independently associated with clinically diagnosed Alzheimer's disease (frequent/severe grade odds ratio 6.26, 95% confidence interval 1.66–23.58; $P = 0.017$, compared with none/mild grade), whereas the severity of MRI-visible perivascular spaces in the basal ganglia was associated with clinically diagnosed subcortical vascular cognitive impairment and negatively predicted Alzheimer's disease (frequent/severe grade odds ratio 0.03, 95% confidence interval 0.00–0.44; $P = 0.009$, compared with none/mild grade). MRI-visible perivascular space severity in either location did not predict PiB-PET. These findings provide further evidence that the anatomical distribution of MRI-visible perivascular spaces may reflect the underlying cerebral small vessel disease. Using MRI-visible perivascular space location and severity together with other imaging markers may improve the diagnostic value of neuroimaging in memory clinic populations, in particular in differentiating between clinically diagnosed Alzheimer's and subcortical vascular cognitive impairment.

1 UCL Stroke Research Centre, Department of Brain Repair and Rehabilitation, UCL Institute of Neurology and the National Hospital for Neurology and Neurosurgery, Russell Square House, 10–12 Russell Square, London WC1B 5EH, UK
2 Department of Neurology, Sungkyunkwan University School of Medicine, Samsung Medical Center, Seoul, Korea
3 Neuroscience Center, Samsung Medical Center, Seoul, Korea

Received July 13, 2016. Revised October 10, 2016. Accepted December 4, 2016. Advance Access publication February 17, 2017

4 Biostatistics Group, University College London Hospitals and University College London Research Support Centre, University College London, Gower Street, London, WC1E 6BT, UK
5 Neuroradiological Academic Unit, Department of Brain Repair and Rehabilitation, UCL Institute of Neurology and the National Hospital for Neurology and Neurosurgery, London, WC1N 3BG, UK

Correspondence to: Professor David J. Werring
UCL Stroke Research Centre,
Department of Brain Repair and Rehabilitation,
UCL Institute of Neurology,
Russell Square House,
10–12 Russell Square,
London, WC1B 5EH, UK
E-mail: d.werring@ucl.ac.uk

Keywords: perivascular space; Alzheimer's disease; subcortical vascular cognitive impairment; cerebral amyoid angiopathy; amyloid PET

Abbreviations: ADCI = Alzheimer's disease-related cognitive impairment; BG = basal ganglia; CAA = cerebral amyloid angiopathy; CSO = centrum semi-ovale; MCI = mild cognitive impairment; PiB = Pittsburgh compound B; PVS = MRI-visible perivascular spaces; SVCI = subcortical vascular cognitive impairment; WMH = white matter hyperintensities

Introduction

Small vessel diseases of the brain are an important cause of stroke and dementia (Pantoni, 2010; Bath and Wardlaw, 2015). Our ability to accurately identify these diseases using neuroimaging markers has improved considerably in recent years (Wardlaw *et al.*, 2013*b*), with increasing interest in the role of small vessel pathology in traditionally 'non-vascular' dementias, such as Alzheimer's disease. The most common age-related cerebral small vessel disease subtypes are: arteriolosclerosis and related processes affecting deep perforating arteries (often termed hypertensive arteriopathy); and cerebral amyloid angiopathy (CAA) (Pantoni, 2010). Arteriolosclerosis is associated with hypertension, diabetes and increasing age, and 'vascular' dementia (the most common form of which is subcortical vascular cognitive impairment, SVCI), whereas CAA is the result of amyloid-β deposition in the walls of small to medium vessels in the cortex and leptomeninges, and found in over 90% of those with Alzheimer's disease (Charidimou *et al.*, 2012). As well as being a risk factor for spontaneous intracerebral haemorrhage (Samarasekera *et al.*, 2012), CAA can result in cognitive deficits independently of Alzheimer's disease (Arvanitakis *et al.*, 2011; Boyle *et al.*, 2015; Reijmer *et al.*, 2015), although the exact interaction between these two processes remains unclear. Traditionally Alzheimer's disease and SVCI have been described as having distinct neuroimaging profiles (Wardlaw *et al.*, 2013*b*; Greenberg *et al.*, 2014), but clinically differentiating between the two remains difficult, as both the cognitive symptoms and the imaging findings frequently overlap (Lee *et al.*, 2011, 2014; Wardlaw *et al.*, 2013*a*, *b*; Greenberg *et al.*, 2014). Given this, identifying new markers that further improve our ability to discriminate between Alzheimer's disease and SVCI remains both relevant and important, in particular with regard to recruitment for clinical trials investigating pharmacological interventions (Ahmed *et al.*, 2014; Andrieu *et al.*, 2015).

MRI-visible perivascular spaces (PVS)—sometimes termed Virchow-Robin spaces, type 3 lacunes and *état crible*—are hypothesized to result from an enlargement of the potential space within the wall of a cerebral blood vessel, possibly secondary to impaired interstitial fluid drainage (Wardlaw *et al.*, 2013*b*; Weller *et al.*, 2015). Whereas enlargement in the basal ganglia (BG-PVS) appears to be associated with markers of arteriolosclerosis, enlargement of PVS in the white matter centrum semi-ovale (CSO-PVS) appears to be associated with cerebral amyloid-β pathologies, both Alzheimer's disease and CAA (Charidimou *et al.*, 2013, 2014*b*; Martinez-Ramirez *et al.*, 2013). Neuropathological studies have demonstrated that the frequency and severity of white matter PVS is greater in Alzheimer's disease than controls, and this was associated with brain amyloid-β load, severity of CAA and apolipoprotein E (*APOE*) ε4 presence (Roher *et al.*, 2003). The association between Alzheimer's disease and increased white matter PVS volume has also been demonstrated using neuroimaging (Ramirez *et al.*, 2015). CSO-PVS are associated with CAA-related intracerebral haemorrhage (Charidimou *et al.*, 2013, 2014*b*) and its 'haemorrhagic' markers, namely lobar microbleeds (Martinez-Ramirez *et al.*, 2013; Yakushiji *et al.*, 2014) and cortical superficial siderosis (Charidimou *et al.*, 2014*a*). Indeed, a recent study using post-mortem 7 T magnetic resonance in CAA-related intracerebral haemorrhage found an association between juxta-cortical PVS enlargement and the histopathological grade of CAA in the overlying cortex (van Veluw *et al.*, 2016). In addition, a small study of patients with CAA-related intracerebral haemorrhage and healthy controls found an association between amyloid-PET burden (as measured using ^{11}C-Pittsburgh compound B, PiB) and CSO-PVS (Charidimou *et al.*, 2015). This makes PVS topography in certain clinical contexts a

promising new marker of cerebral small vessel diseases. However, the relationships between PVS topography, amyloid deposition and clinical dementia syndromes (Alzheimer's disease and SVCI) are not well understood.

We aimed to further evaluate this association of PVS location with small vessel disease type in a cohort of patients with Alzheimer's disease related cognitive impairment (ADCI; either Alzheimer's disease or Alzheimer's disease mild cognitive impairment) and SVCI (either subcortical vascular dementia or subcortical vascular mild cognitive impairment). We hypothesized that ADCI is associated with CSO-PVS (as these patients are likely to have CAA), but not BG-PVS, which instead is associated with SVCI (and arteriolosclerosis). We also hypothesized that, given that CSO-PVS are associated with cerebral amyloid-β diseases, CSO-PVS is associated with PiB positivity, whereas BG-PVS would not demonstrate any such association.

Materials and methods

Participants

We prospectively recruited 251 subjects with cognitive impairment who underwent PiB-PET and structural brain MRI, between July 2007 and July 2011. We included 45 patients with amnestic mild cognitive impairment (MCI), 69 with probable Alzheimer's disease dementia, 67 with subcortical vascular MCI, and 70 with subcortical vascular dementia; all patients had been clinically diagnosed at Samsung Medical Center. Of these, 226 subjects were included in the current study, with exclusions made either due to imaging being unavailable ($n = 20$) or too degraded by motion artefact to be interpreted ($n = 5$). Probable Alzheimer's disease dementia patients fulfilled diagnostic criteria proposed by the National Institute of Neurological and Communicative Disorders and Stroke and the Alzheimer's disease and Related Disorders Association (NINCDS-ADRDA) (McKhann *et al.*, 1984). Patients with subcortical vascular dementia met the diagnostic criteria for vascular dementia as determined by the Diagnostic and Statistical Manual of Mental Disorders (Fourth Edition), and also fulfilled the imaging criteria for subcortical vascular dementia proposed by Erkinjuntti *et al.* (2000). Patients with amnestic MCI and subcortical vascular MCI met Petersen's criteria for MCI with modifications (Seo *et al.*, 2009). All subcortical vascular MCI and subcortical vascular dementia patients had severe white matter hyperintensities (WMH) on their MRI scans, which was defined as a cap or band (periventricular WMH) $\geqslant 10$ mm and deep white matter lesions (deep WMH) $\geqslant 25$ mm, as modified from the Fazekas ischaemia criteria (Fazekas *et al.*, 1993). All patients with amnestic MCI and patients with Alzheimer's disease were classified as having minimal (periventricular WMH < 5 mm and deep WMH < 5 mm) or moderate WMH (between minimal and severe grades). These WMH definitions are in line with those recently proposed to describe WMH of presumed vascular origin (Wardlaw *et al.*, 2013*b*). Patients with amnestic MCI or Alzheimer's disease were considered to have ADCI, whereas those with subcortical vascular MCI or subcortical vascular dementia were considered to have SVCI. We excluded patients with territorial infarctions and those with WMHs due to radiation injury, multiple sclerosis, vasculitis, or leukodystrophy. All patients completed a clinical interview and neurological examination. Blood tests included a complete blood count, blood chemistry test, vitamin B_{12}/folate measurement, syphilis serology, thyroid function test, and *APOE* genotyping.

We obtained written consent from each patient, and the study protocol was approved by the Institutional Review Board of the Samsung Medical Center.

PiB-PET acquisition and data analysis

^{11}C-PiB-PET scanning was performed on all participants at Samsung or Asan Medical Center using a Discovery STe PET/CT scanner (GE Medical Systems) in 3D scanning mode that examined 35 slices of 4.25 mm thickness spanning the entire brain. ^{11}C-PiB was injected into an antecubital vein as a bolus with a mean dose of 420 MBq (i.e. range 259–550 MBq). A CT scan was performed for attenuation correction 60 min after injection. A 30-min emission static PET scan was then initiated. The specific radioactivity of ^{11}C-PiB at the time of administration was >1500 Ci/mmol for patients and the radiochemical yield was $>35\%$. The radiochemical purity of the tracer was $>95\%$ in all PET studies.

PiB-PET images were co-registered to individual MRIs, which were normalized to a T_1-weighted MRI template. Using these parameters, MRI co-registered PiB-PET images were normalized to the MRI template. The quantitative regional values of PiB retention on the spatially normalized PiB images were obtained by an automated volumes of interest analysis using the automated anatomical labeling (AAL) atlas. Data processing was performed using SPM Version 5 (SPM5) within Matlab 6.5 (MathWorks, Natick, MA).

To measure PiB retention, we used the cerebral cortical region to cerebellum uptake ratio. The cerebellum was used as a reference region as it did not show group differences. We selected 28 cortical volumes of interest from left and right hemispheres using the AAL atlas. The cerebral cortical volumes of interest that were chosen for this study consisted of the bilateral frontal (superior and middle frontal gyri, the medial portion of superior frontal gyrus, the opercular portion of inferior frontal gyrus, the triangular portion of inferior frontal gyrus, supplementary motor area, orbital portion of the superior, middle, and inferior orbital frontal gyri, rectus and olfactory cortex), posterior cingulate gyri, parietal (superior and inferior parietal, supramarginal and angular gyri, and precuneus), lateral temporal (superior, middle and inferior temporal gyri, and heschl gyri), and occipital (superior, middle, and inferior occipital gyri, cuneus, calcarine fissure, and lingual and fusiform gyri). Regional cerebral cortical uptake ratios were calculated by dividing each cortical volume of interest uptake ratio by the mean uptake of the cerebellar cortex (cerebellum crus1 and crus2). Global PiB uptake ratio was calculated from the volume-weighted average uptake ratio of bilateral 28 cerebral cortical volumes of interest. Patients were considered PiB-positive if their global PiB retention ratio was over 1.5 from the mean for normal controls (Lee *et al.*, 2011).

MRI acquisition

Standardized T_1, T_2, T_2^* gradient echo (GRE), and 3D fluid-attenuated inversion recovery (FLAIR) images were acquired from all subjects at Samsung Medical Center using the same 3 T MRI scanner (Philips 3.0T Achieva). In all subjects, these images were obtained in one session and all MRIs were obtained in the same orientation and slice positions. T_2^* GRE-MRI were obtained using the following parameters: axial slice thickness, 5.0 mm; interslice thickness, 2 mm; repetition time, 669 ms; echo time 16 ms; flip angle, 18°, and matrix size of 560 × 560 pixels. We acquired the 3D FLAIR images with the following imaging parameters: axial slice thickness of 2 mm; no gap; repetition time of 11 000 ms; echo time of 125 ms; flip angle of 90°; and matrix size of 512 × 512 pixels.

Measurement of white matter hyperintensity volume

WMH volume (in millilitres) was quantified on FLAIR images using an automated method (Jeon *et al.*, 2011). Because the contrasting properties of FLAIR images allow automated segmentation and classification of WMH (Sachdev *et al.*, 2004), we used FLAIR images to quantify WMH. The procedures for measuring regional WMH volume have been previously described (Jeon *et al.*, 2011). First, we extracted the WMH candidate regions using T_1-weighted images to avoid misclassification in the subarachnoid space and CSF interface, which cannot be excluded by intensity threshold or the conventional brain extraction tools. Second, to extract WMH, a threshold method was applied to the FLAIR images after using the WMH candidate mask. Even though the threshold value was selected after intensity normalization, segmented results could contain the false positive or negative depending on the extent of WMH. Therefore, if the results were found to contain an error, the threshold value was reselected through visual inspection by two raters.

Lacune assessment on MRI

A lacune was defined as a lesion $\geqslant$3 mm and $\leqslant$15 mm in diameter with low signal on T_1 imaging, high signal on T_2-weighted imaging, and with a perilesional halo on FLAIR imaging. Two experienced neurologists who were blinded to the patients' clinical data reviewed the number and location of the lacunes on 80 axial FLAIR slices. This meets the recently proposed definition of a lacune of presumed vascular origin (Wardlaw *et al.*, 2013*b*). Two neurologists manually counted the number of lacunes, with a kappa value of 0.78.

Analysis of cerebral microbleeds on gradient echo MRI

Cerebral microbleeds were defined as lesions $\leqslant$10 mm in diameter and were also defined using criteria proposed by Greenberg *et al.* (2009). Two experienced neurologists, who were blinded to patient data, reviewed the number and location of cerebral microbleeds on 20 T_2 GRE-MRI axial slices. The two neurologists had an agreement kappa value for the presence of cerebral microbleeds of 0.92, and a consensus was reached in any case of discrepancy.

Cerebral microbleeds were counted in four lobar regions (frontal, temporal, parietal, occipital) and also in deep brain regions. A lobar region was defined as tissue $\leqslant$10 mm from the brain surface.

Quantification of MRI-visible perivascular spaces

PVS were defined and rated on axial T_2-weighted MRIs, according to STandards for ReportIng Vascular changes on nEuroimaging (STRIVE) (Wardlaw *et al.*, 2013*b*), by a trained observer who was blinded to the clinical information (G.B.) using a validated 4-point visual rating scale (0, no PVS; 1, <10 PVS; 2, 11–20 PVS; 3, 21–40 PVS; and 4, >40 PVS) in the basal ganglia and centrum semi-ovale (cerebral hemisphere white matter) (Maclullich *et al.*, 2004; Doubal *et al.*, 2010). Rating was carried out on a single predefined slice (first slice above the anterior commissure in the basal ganglia; the first slice above the level of the lateral ventricles for the centrum semi-ovale). Both hemispheres were counted, and the hemisphere with the highest score was recorded. Severity was defined as 'none/mild' (equivalent to rating scale categories 0 and 1), 'moderate' (rating scale category 2), and 'frequent/severe' (rating scale categories 3 and 4) to generate groups of a similar size for meaningful subsequent statistical analysis. Figure 1 demonstrates PVS examples of each severity grade in both locations.

Statistical analysis

Baseline characteristics were compared using chi-squared or Fisher's exact tests for categorical variables, independent *t*-tests for normally distributed continuous variables and Mann-Whitney U-tests for continuous variables that were not normally distributed. PVS (both CSO-PVS and BG-PVS) were considered as categorical variables, subdivided by severity as described above. Univariable and multivariable logistic regression analyses were performed; variables of interest in univariable analysis were included in the multivariable models. WMH volume was not included in the analysis for predictors of diagnosis, as it had been used to make the original clinical diagnosis.

Statistical analysis was performed with Stata (Version 11.2).

Results

MRI-visible perivascular space topography as a predictor of clinical diagnosis

The comparison of baseline characteristics of the ADCI and SVCI groups are shown in Table 1. Those in the ADCI group were younger (mean 70.3 years versus 73.8 years, $P = 0.0012$), more likely to be PiB-positive (78.2% versus 29.3%, $P < 0.0001$) and carry the *APOE* ε4 allele (48.6% versus 25.7%, $P < 0.0001$). Those in the SVCI group were more likely to have hypertension (77.6% versus 47.3%, $P < 0.0001$), diabetes mellitus (25.9% versus 13.6%,

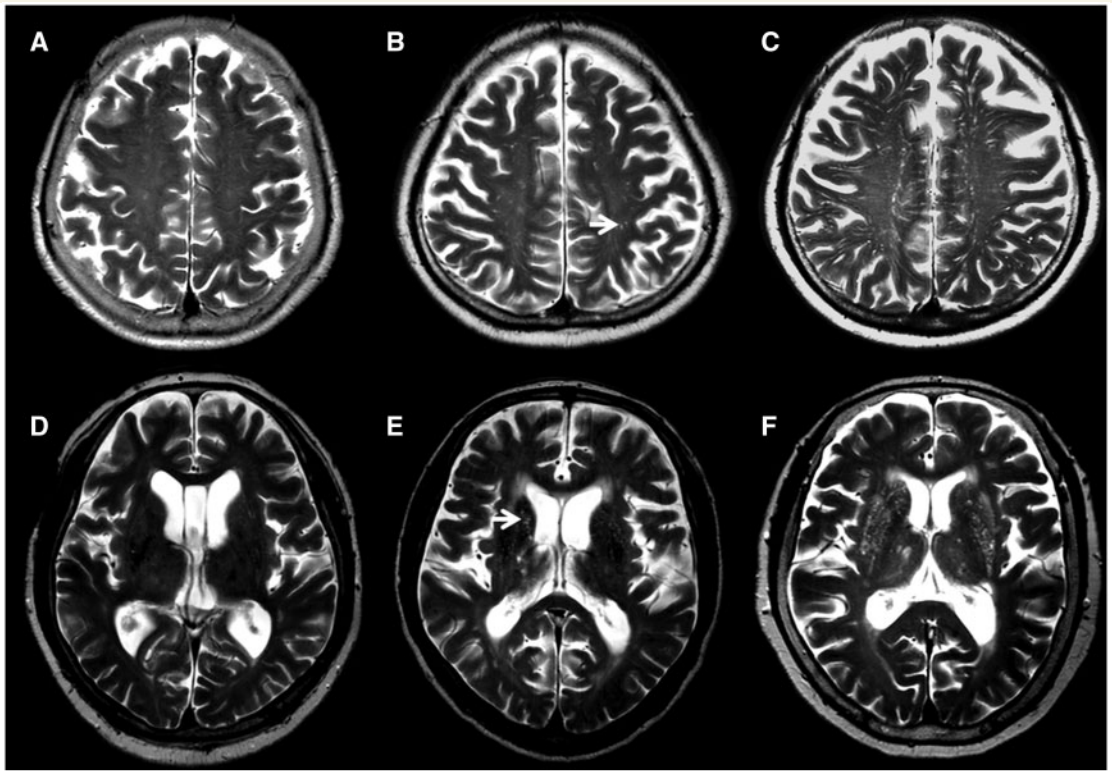

Figure 1 Examples of MRI-visible perivascular spaces. (**A–C**) Examples of MRI-visible CSO-PVS. (**A**) None/mild grade, (**B**) moderate grade, (**C**) frequent/severe grade. (**D–F**) Examples of MRI-visible BG-PVS. (**D**) None/mild grade, (**E**) moderate grade, (**F**) frequent/severe grade.

Table 1 Baseline characteristics according to disease classification (*p*-values reflect comparisons between ADCI and SVCI groups using Chi-squared, Fishers exact, independent *t*-tests or Mann-Whitney U-tests as appropriate).

	All	ADCI	SVCI	*P*-value
n (%)	226	110 (48.7%)	116 (51.3%)	-
Age, years, mean (SD)	72.1 (8.1)	70.3 (8.8)	73.8 (7.0)	0.0012
Sex, male, *n* (%)	98 (43.4%)	49 (44.6%)	49 (42.3%)	0.727
Hypertension, *n* (%)	142 (62.8%)	52 (47.3%)	90 (77.6%)	<0.0001
Diabetes mellitus, *n* (%)	45 (19.9%)	15 (13.6%)	30 (25.9%)	0.021
Hyperlipidaemia, *n* (%)	68 (30.1%)	26 (23.6%)	42 (36.2%)	0.039
Prior stroke, *n* (%)	37 (16.4%)	6 (5.4%)	31 (26.7%)	<0.0001
PiB positivity, *n* (%)	120 (53.1%)	86 (78.2%)	34 (29.3%)	<0.0001
Presence of *APOE* ε2, *n* (%)	22 (10.0%)	7 (6.5%)	15 (13.3%)	0.096
Presence of *APOE* ε3, *n* (%)	203 (92.3%)	93 (86.9%)	110 (97.4%)	0.004
Presence of *APOE* ε4, *n* (%)	81 (36.8%)	52 (48.6%)	29 (25.7%)	<0.0001
Lacunes, median (IQR%)	1 (0–9)	0 (0–0)	9 (3.5–17)	<0.0001
cSS presence, *n* (%)	8 (3.5%)	5 (4.6%)	3 (2.6%)	0.426
Strictly lobar CMB (presence), *n* (%)	17 (7.5%)	7 (6.4%)	10 (8.6%)	0.520
Deep CMB (presence), *n* (%)	69 (30.8%)	7 (6.5%)	62 (53.5%)	<0.0001
CSO-PVS				
None/mild (grade 0–1), *n* (%)	73 (32.3%)	16 (14.6%)	57 (49.1%)	<0.0001
Moderate (grade 2), *n* (%)	91 (40.3%)	49 (44.6%)	42 (36.2%)	
Frequent/severe (grade 3–4), *n* (%)	62 (27.4%)	45 (40.9%)	17 (14.7%)	
BG-PVS				
None/mild (grade 0–1), *n* (%)	170 (75.2%)	103 (93.6%)	67 (57.57%)	<0.0001
Moderate (grade 2), *n* (%)	44 (19.5%)	6 (5.4%)	38 (32.8%)	
Frequent/severe (grade 3–4), *n* (%)	12 (5.3%)	1 (0.91%)	11 (9.48%)	

ADCI = Alzheimer's disease related cognitive impairment; *APOE* = Apolipoprotein E; BG = Basal ganglia; CSO = Centrum semi-ovale; cSS = Cortical superficial siderosis; CMB = Cerebral microbleed; IQR = Interquartile range; PiB = 11-Carbon based Pittsburgh compound B; PVS = Perivascular space (MRI-visible); SD = Standard deviation; SVCI = Subcortical vascular cognitive impairment.

Table 2 Logistic regression analysis for predictors of clinical diagnosis (ADCI group)

	Univariable		Multivariable (CSO)		Multivariable (BG)	
	OR (95% CI)	*P*-value	OR (95% CI)	*P*-value	OR (95% CI)	*P*-value
CSO-PVS		<0.00001		0.017	-	-
None/mild (grade 0–1)	Reference group		Reference group			
Moderate (grade 2)	4.16 (2.08–8.29)		3.57 (1.17–10.89)			
Frequent / Severe (grade 3–4)	9.43 (4.29–20.71)		6.26 (1.66–23.58)			
BG-PVS		<0.00001	-	-		0.009
None/mild (grade 0–1)	Reference group				Reference group	
Moderate (grade 2)	0.10 (0.04–0.26)				0.26 (0.07–1.01)	
Frequent/severe (grade 3–4)	0.06 (0.01–0.47)				0.03 (0.00–0.44)	
Age (for each year older)	0.95 (0.91 to 0.98)	0.002	0.94 (0.88 to 1.01)	0.091	0.95 (0.88 to 1.03)	0.214
Hypertension (presence)	0.26 (0.15 to 0.46)	<0.0001	1.13 (0.39 to 3.28)	0.828	1.04 (0.35 to 3.11)	0.951
Diabetes (presence)	0.45 (0.23 to 0.90)	0.023	0.45 (0.14 to 1.44)	0.180	0.42 (0.13 to 1.36)	0.149
Hyperlipidaemia (presence)	0.55 (0.31 to 0.97)	0.041	0.39 (0.14 to 1.11)	0.077	0.53 (0.18 to 1.55)	0.247
Prior stroke (presence)	0.16 (0.06 to 0.40)	<0.0001	0.55 (0.12 to 2.56)	0.444	0.53 (0.12 to 2.28)	0.396
PiB positivity (presence)	8.64 (4.72 to 15.81)	<0.0001	3.97 (1.46 to 10.80)	0.007	5.63 (1.96 to 16.21)	0.001
APOE ε2 (presence)	0.46 (0.18 to 1.17)	0.103	-	-	-	-
APOE ε3 (presence)	0.18 (0.05 to 0.65)	0.009	0.47 (0.05 to 4.31)	0.507	0.29 (0.03 to 2.73)	0.277
APOE ε4 (presence)	2.73 (1.55 to 4.83)	0.001	0.82 (0.28 to 2.40)	0.722	0.65 (0.21 to 1.99)	0.449
Lacunes (per additional lacune)	0.49 (0.39 to 0.61)	<0.0001	0.61 (0.48 to 0.78)	<0.0001	0.59 (0.47 to 0.75)	<0.0001
cSS (presence)	1.79 (0.42 to 0.69)	0.432	-	-	-	-
Strictly lobar CMB (presence)	0.72 (0.26 to 1.96)	0.522	-	-	-	-
Deep CMB (presence)	0.06 (0.03 to 0.14)	<0.0001	0.45 (0.11 to 1.75)	0.247	0.59 (0.14 to 2.54)	0.478

cSS = cortical superficial siderosis; CMB = cerebral microbleed.

$P = 0.021$), hyperlipidaemia (36.2% versus 23.6%, $P = 0.039$), and prior stroke (26.7% versus 5.4%, $P < 0.0001$). They were also more likely to carry the *APOE* ε3 allele (97.4% versus 86.9%, $P = 0.004$) and have lacunes (median 9 versus 0, $P < 0.0001$) and deep cerebral microbleeds (53.5% versus 6.5%, $P < 0.0001$).

In univariable logistic regression analysis, increasing CSO-PVS severity was a positive predictor of ADCI; individuals with moderate CSO-PVS had an odds ratio (OR) of 4.16 [95% confidence interval (CI): 2.08–8.29] and those with frequent/severe CSO-PVS had an OR of 9.43 (95% CI: 4.29–20.71) compared to those with none/mild CSO-PVS (Table 2). Increasing severity of BG-PVS was negatively associated with ADCI (i.e. positively associated with a clinical diagnosis of SVCI); individuals with moderate BG-PVS had an OR for ADCI of 0.10 (95% CI: 0.04–0.26) and those with frequent/severe BG-PVS had an OR of 0.06 (95% CI: 0.01–0.47) compared to those with none/mild BG-PVS. After adjustment for other confounding variables, all of these associations remained: increasing CSO-PVS severity was a positive predictor of clinically diagnosed ADCI (none/mild as reference group: moderate severity, OR 3.57, 95% CI 1.17–10.89; frequent/severe, OR 6.26, 95% CI 1.66–23.58). Increasing severity of BG-PVS was negatively associated with ADCI and thus predictive of clinically diagnosed SVCI (none/mild as reference group: moderate severity, OR 0.26, 95% CI 0.07–1.01); frequent/severe, OR 0.03, 95% CI 0.00–0.44). PiB positivity and number of lacunes were also associated with a diagnosis of ADCI after adjustment.

MRI-visible perivascular space topography as a predictor of PiB positivity

The baseline characteristics of the PiB positive and negative groups are given in Table 3. Those in the PiB-positive group were more likely to have a diagnosis of ADCI (71.7% versus 22.6%, $P < 0.0001$), carry the *APOE* ε4 allele (53.9% versus 17.5%, $P < 0.0001$) and have cortical superficial siderosis, although the numbers were small (5.8% versus 0.9%, $P = 0.047$). They were less likely to have hypertension (50.0% versus 77.4%, $P < 0.0001$), diabetes mellitus (15.0% versus 25.5%, $P = 0.049$), previous stroke (8.3% versus 25.5%, $P = 0.001$) and the *APOE* ε3 allele (86.3% versus 99.0%, $P < 0.0001$). They had a lower WMH volume (median 5.2 ml versus 29.9 ml, $P < 0.00001$), fewer lacunes (median 0 versus 7, $P < 0.00001$) and a lower presence of deep microbleeds (16.8% versus 46.7%, $P < 0.0001$).

In univariable logistic regression analysis increasing CSO-PVS severity was a positive predictor of PiB positivity; individuals with moderate CSO-PVS had an OR of 1.37 (95% CI: 0.74–2.54) and those with frequent/severe CSO-PVS had an OR of 2.50 (95% CI: 1.24–5.04) compared to those with none/mild CSO-PVS, respectively (Table 4). However, after adjustment for other factors, there was no relationship between CSO-PVS severity and PiB positivity. BG-PVS severity was not associated with PiB positivity. The only variables that remained independently associated with

Table 3 Baseline characteristics for PiB positive and negative groups

	PiB negative (retention ratio < 1.5)	PiB positive (retention ratio ⩾ 1.5)	*P*-value
n (%)	106 (46.9)	120 (53.1)	-
Age, years, mean (SD)	72.0 (7.2)	72.2 (8.8)	0.808
Sex, male, *n* (%)	48 (45.3)	50 (41.7)	0.584
Hypertension, *n* (%)	82 (77.4)	60 (50.0)	<0.0001
Diabetes mellitus, *n* (%)	27 (25.5)	18 (15.0)	0.049
Hyperlipidaemia, *n* (%)	37 (34.9)	31 (25.8)	0.138
Prior stroke, *n* (%)	27 (25.5)	10 (8.3)	0.001
ADCI, *n* (%)	24 (22.6)	86 (71.7)	<0.0001
SVCI, *n* (%)	82 (77.4)	34 (28.3)	<0.0001
Presence of *APOE* ε2, *n* (%)	14 (13.6)	8 (6.8)	0.096
Presence of *APOE* ε3, *n* (%)	102 (99.0)	101 (86.3)	<0.0001
Presence of *APOE* ε4, *n* (%)	18 (17.5)	63 (53.9)	<0.0001
WMH volume, ml, median (IQR)	29.9 (13.6–45.5)	5.2 (1.2–26.2)	<0.00001
Lacunes, median (IQR)	7 (1–17)	0 (0–2)	<0.00001
cSS presence, *n* (%)	1 (0.9)	7 (5.8)	0.047
Strictly lobar CMB (presence), *n* (%)	7 (6.6)	10 (8.3)	0.623
Deep CMB (presence), *n* (%)	49 (46.7)	20 (16.8)	<0.0001
CSO-PVS			
None/mild (grade 0–1), *n* (%)	41 (38.7)	32 (26.7)	0.033
Moderate (grade 2), *n* (%)	44 (41.5)	47 (39.2)	
Frequent/severe (grade 3–4), *n* (%)	21 (19.8)	41 (34.2)	
BG-PVS			
None/mild (grade 0–1), *n* (%)	76 (71.7)	94 (78.3)	0.480
Moderate (grade 2), *n* (%)	23 (21.7)	21 (17.5)	
Frequent/severe (grade 3–4), *n* (%)	7 (6.6)	5 (4.2)	

P-values reflect comparisons between PiB positive and negative groups using chi-squared, Fishers exact, independent *t*-tests or Mann-Whitney U-tests as appropriate. cSS = cortical superficial siderosis; CMB = cerebral microbleed.

Table 4 Logistic regression analysis for predictors of PiB positivity

	Univariable		Multivariable	
	OR (95% CI)	*P*-value	OR (95% CI)	*P*-value
CSO-PVS		0.032		0.607
None/mild (grade 0–1)	Reference group		Reference group	
Moderate (grade 2)	1.37 (0.74–2.54)		0.67 (0.29–1.59)	
Frequent/severe (grade 3–4)	2.50 (1.24–5.04)		0.93 (0.35–2.46)	
BG-PVS		0.480	-	-
None/mild (grade 0–1)	Reference group			
Moderate (grade 2)	0.74 (0.38–1.43)			
Frequent/severe (grade 3–4)	0.58 (0.18–1.89)			
Hypertension (presence)	0.29 (0.16–0.52)	<0.0001	0.52 (0.24–1.10)	0.085
Diabetes (presence)	0.52 (0.27–1.00)	0.051	0.97 (0.42–2.26)	0.947
Previous stroke (presence)	0.27 (0.12–0.58)	0.001	0.48 (0.17–1.33)	0.157
ADCI diagnosis	8.64 (4.72–15.81)	<0.0001	7.56 (2.59–22.46)	<0.0001
APOE ε2 (presence)	0.47 (0.19–1.16)	0.102	-	-
APOE ε3 (presence)	0.06 (0.01–0.48)	0.007	0.25 (0.03–2.29)	0.221
APOE ε4 (presence)	5.51 (2.95–10.29)	<0.0001	3.87 (1.80–8.32)	0.001
WMH volume (for each ml higher)	0.97 (0.96–0.98)	<0.0001	1.03 (1.00–1.05)	0.055
Lacunes (for one number higher)	0.88 (0.83–0.92)	<0.0001	0.94 (0.88–0.99)	0.026
cSS (presence)	6.50 (0.79–53.76)	0.082	-	-
Strictly lobar CMB (presence)	1.29 (0.47–3.51)	0.623	-	-
Deep CMB (presence)	0.23 (0.12–0.43)	<0.0001	1.07 (0.43–2.65)	0.886

cSS = cortical superficial siderosis; CMB = cerebral microbleed.

PiB positivity were ADCI diagnosis, presence of the *APOE* ε4 allele and number of lacunes.

Discussion

CSO-PVS severity is strongly associated with clinically diagnosed ADCI whereas BG-PVS severity predicts clinically diagnosed SVCI. However, CSO-PVS severity was not independently associated with PiB positivity. There are two possible interpretations of this lack of independent association between CSO-PVS with PiB amyloid retention: either CSO-PVS are associated with ADCI as a marker of amyloid pathology that cannot be accurately resolved by amyloid-PET, or CSO-PVS are indicative of an amyloid-independent pathology.

Our findings are consistent with previous findings of an association between CSO-PVS and both Alzheimer's disease and CAA, both of which are associated with amyloid-β deposition (Charidimou *et al.*, 2012). One reason for the apparent lack of independent association between CSO-PVS and PiB might be that PiB-PET is unable to resolve smaller blood vessels affected by CAA. This is supported by neuropathological evidence that, although severity of CAA does appear associated with CSO-PVS in Alzheimer's disease, the CAA affected vessels are predominantly less than 500 μm in diameter, which may be too small to be identified using PiB-PET (Roher *et al.*, 2003). Alternatively, the PiB-PET signal observed in our ADCI cohort may be more a measure of parenchymal amyloid-β (this being the predominant signal) and be unrepresentative of the true vascular amyloid-β; PiB-PET binding has been shown to be lower in patients with CAA compared to those with Alzheimer's disease (Johnson *et al.*, 2007). Thus it is possible that any sequelae of vascular amyloid deposition, for example impaired interstitial fluid drainage secondary to a failure to adequately clear pathological proteins, could still be visible as MRI-visible CSO-PVS (Weller *et al.*, 2015), independently of PiB positivity.

An alternative explanation is that CSO-PVS are associated with ADCI but not PiB positivity because they are manifestations of an amyloid-independent process, for example a tau protein-related process. As well as being a core neuropathological finding in Alzheimer's disease, neurofibrillary tangles have been demonstrated in association with CAA in patients with Alzheimer's disease (Jeynes and Provias, 2006), and tau deposits (neurofibrillary tangles and pretangles) have been described in amyloid-β-related angiitis, an inflammatory form of CAA (Kurian *et al.*, 2012). One study reviewing perivascular hyperphosphorylated tau in patients with Alzheimer's disease found higher levels surrounding the CAA affected vessels than the unaffected ones (Williams *et al.*, 2005). Thus it is possible that CAA could impair perivascular drainage, leading to tau aggregation, which could further impair perivascular drainage leading to further tau aggregation and so on (a 'feed-forward' loop), with MRI-visible perivascular spaces being the end result (Weller *et al.*, 2009; Love and Miners, 2015). In animal models, traumatic brain injury appears to disrupt normal perivascular clearance for at least 28 days, resulting in the accumulation of hyper-phosphorylated tau (Iliff *et al.*, 2014); CAA could impair perivascular drainage in a similar way. Alternatively CAA may disrupt perivascular drainage via perturbations in normal arteriolar pulsation (Hawkes *et al.*, 2014; Kress *et al.*, 2014). It is also possible that the presence of hyper-phosphorylated tau has direct deleterious consequences for perivascular astrocytes, for example by directly disrupting their microtubular structure, or altering the expression or localization of membrane channels (for example, aquaporin 4) that change normal interstitial fluid dynamics, with the eventual outcome of an enlarged perivascular space (Arima *et al.*, 1998; Thrane *et al.*, 2014; Iqbal *et al.*, 2016).

This study has some limitations. First, this is an observational study without healthy aged matched controls for comparison; despite this, our findings are generally in keeping with previous reports from Alzheimer's disease and SVCI cohorts. A previous study (Charidimou *et al.*, 2015) has demonstrated an association between PiB positivity and CSO-PVS across a cohort including healthy controls (both aged over and under 60 years) and patients with CAA-related intracerebral haemorrhage; interestingly although those with CAA had a higher burden of CSO-PVS compared with the healthy control groups ($P = 0.08$), there did not appear to be a difference in PiB positivity between healthy older patients and CAA ($P = 0.53$). This may provide further evidence that CSO-PVS burden is a closer correlate of vascular amyloid burden than PiB-PET measures are, but it is difficult to draw firm conclusions as this study included only 31 participants (Charidimou *et al.*, 2015). Additionally, our findings may only be applicable to a selected memory clinic population, specifically those with either Alzheimer's disease-related cognitive impairment or SVCI, rather than the full spectrum of dementia syndromes. Our project would also have strengthened if participants had other measures of amyloid-β burden in addition to amyloid-PET, for example quantification of CSF or serum amyloid-β. Certain measures, for example the ratio of amyloid-β_{40}:amyloid-β_{42} (Verbeek *et al.*, 2009), may better capture vascular amyloid-β and thus might demonstrate an association with CSO-PVS. It was not possible to draw any conclusions on whether the association between Alzheimer's disease diagnosis and CSO-PVS severity was due to any form of CAA. Only small numbers within our cohort had characteristics known to be associated with haemorrhage-associated CAA (type 2), namely an *APOE* ε2 allele (notably, none of the cohort were homozygous for *APOE* ε2), strictly lobar microbleeds and cSS; however, given that over 95% of those with Alzheimer's disease have pathological evidence of CAA it may be that the predominant CAA subtype in Alzheimer's disease is type 1, which is associated with *APOE* ε4 and capillary level disease (Charidimou *et al.*, 2012). Thus it may be the case that

more traditional 'haemorrhagic' markers of CAA are of less clinical relevance in this population.

This study provides further supporting evidence that CSO-PVS are a key imaging marker for Alzheimer's disease, but without being a measure of amyloid positivity as measured by PiB-PET. This raises the possibility that CSO-PVS are a measure of vascular amyloid processes that are not identified by amyloid-PET, or alternatively of an amyloid independent process, or both. Future work reviewing the association between CSO-PVS and other circulating biomarkers of amyloid-β burden, and the relationship between tau and CAA will be necessary to further clarify the mechanisms underlying these findings.

Funding

G.B. receives funding from the Rosetrees Trust. H.J.K. receives funding from the National Research Foundation of Korea (NRF-2015R1C1A2A01053281). S.W.S. receives funding from the Brain Research Program through the National Research Foundation of Korea (NRF-2016M3C7A1913844) and the Korea Ministry of Environment (MOE) (2014001360002). D.J.W. receives research support from the Stroke Association, the British Heart Foundation and the Rosetrees Trust.

References

Ahmed RM, Paterson RW, Warren JD, Zetterberg H, O'Brien JT, Fox NC, et al. Biomarkers in dementia: clinical utility and new directions. J Neurol Neurosurg Psychiatry 2014; 85: 1426–34.

Andrieu S, Coley N, Lovestone S, Aisen PS, Vellas B. Prevention of sporadic Alzheimer's disease: lessons learned from clinical trials and future directions. Lancet Neurol 2015; 14: 926–44.

Arima K, Izumiyama Y, Nakamura M, Nakayama H, Kimura M, Ando S, et al. Argyrophilic tau-positive twisted and non-twisted tubules in astrocytic processes in brains of Alzheimer-type dementia: an electron microscopical study. Acta Neuropathol 1998; 95: 28–39.

Arvanitakis Z, Leurgans SE, Wang Z, Wilson RS, Bennett DA, Schneider JA. Cerebral amyloid angiopathy pathology and cognitive domains in older persons. Ann Neurol 2011; 69: 320–7.

Bath PM, Wardlaw JM. Pharmacological treatment and prevention of cerebral small vessel disease: a review of potential interventions. Int J Stroke 2015; 10: 469–78.

Boyle PA, Yu L, Nag S, Leurgans S, Wilson RS, Bennett DA, et al. Cerebral amyloid angiopathy and cognitive outcomes in community-based older persons. Neurology 2015; 85: 1930–6.

Charidimou A, Gang Q, Werring DJ. Sporadic cerebral amyloid angiopathy revisited: recent insights into pathophysiology and clinical spectrum. J Neurol Neurosurg Psychiatry 2012; 83: 124–37.

Charidimou A, Hong YT, Jager HR, Fox Z, Aigbirhio FI, Fryer TD, et al. White matter perivascular spaces on magnetic resonance imaging: marker of cerebrovascular amyloid burden?. Stroke 2015; 46: 1707–9.

Charidimou A, Jager RH, Peeters A, Vandermeeren Y, Laloux P, Baron JC, et al. White matter perivascular spaces are related to cortical superficial siderosis in cerebral amyloid angiopathy. Stroke 2014a; 45: 2930–5.

Charidimou A, Jaunmuktane Z, Baron JC, Burnell M, Varlet P, Peeters A, et al. White matter perivascular spaces: an MRI marker in pathology-proven cerebral amyloid angiopathy?. Neurology 2014b; 82: 57–62.

Charidimou A, Meegahage R, Fox Z, Peeters A, Vandermeeren Y, Laloux P, et al. Enlarged perivascular spaces as a marker of underlying arteriopathy in intracerebral haemorrhage: a multicentre MRI cohort study. J Neurol Neurosurg Psychiatry 2013; 84: 624–9.

Doubal FN, MacLullich AM, Ferguson KJ, Dennis MS, Wardlaw JM. Enlarged perivascular spaces on MRI are a feature of cerebral small vessel disease. Stroke 2010; 41: 450–4.

Erkinjuntti T, Inzitari D, Pantoni L, Wallin A, Scheltens P, Rockwood K, et al. Research criteria for subcortical vascular dementia in clinical trials. J Neural Transm Suppl 2000; 59: 23–30.

Fazekas F, Kleinert R, Offenbacher H, Schmidt R, Kleinert G, Payer F, et al. Pathologic correlates of incidental MRI white matter signal hyperintensities. Neurology 1993; 43: 1683–9.

Greenberg SM, Al-Shahi Salman R, Biessels GJ, van Buchem M, Cordonnier C, Lee JM, et al. Outcome markers for clinical trials in cerebral amyloid angiopathy. Lancet Neurol 2014; 13: 419–28.

Greenberg SM, Vernooij MW, Cordonnier C, Viswanathan A, Al-Shahi Salman R, Warach S, et al. Cerebral microbleeds: a guide to detection and interpretation. Lancet Neurol 2009; 8: 165–74.

Hawkes CA, Jayakody N, Johnston DA, Bechmann I, Carare RO. Failure of perivascular drainage of beta-amyloid in cerebral amyloid angiopathy. Brain Pathol 2014; 24: 396–403.

Iliff JJ, Chen MJ, Plog BA, Zeppenfeld DM, Soltero M, Yang L, et al. Impairment of glymphatic pathway function promotes tau pathology after traumatic brain injury. J Neurosci 2014; 34: 16180–93.

Iqbal K, Liu F, Gong CX. Tau and neurodegenerative disease: the story so far. Nat Rev Neurol 2016; 12: 15–27.

Jeon S, Yoon U, Park JS, Seo SW, Kim JH, Kim ST, et al. Fully automated pipeline for quantification and localization of white matter hyperintensity in brain magnetic resonance image. Int J Imag Syst Tech 2011; 21: 193–200.

Jeynes B, Provias J. The possible role of capillary cerebral amyloid angiopathy in Alzheimer lesion development: a regional comparison. Acta neuropathol 2006; 112: 417–27.

Johnson KA, Gregas M, Becker JA, Kinnecom C, Salat DH, Moran EK, et al. Imaging of amyloid burden and distribution in cerebral amyloid angiopathy. Ann Neurol 2007; 62: 229–34.

Kress BT, Iliff JJ, Xia M, Wang M, Wei HS, Zeppenfeld D, et al. Impairment of paravascular clearance pathways in the aging brain. Ann Neurol 2014; 76: 845–61.

Kurian M, Burkhardt K, Assal F, Kovari E, Horvath J. Amyloid plaques and intraneuronal tau inclusions in A-Beta-Related Angiitis (ABRA). Neuropathol Appl Neurobiol 2012; 38: 391–4.

Lee JH, Kim SH, Kim GH, Seo SW, Park HK, Oh SJ, et al. Identification of pure subcortical vascular dementia using 11C-Pittsburgh compound B. Neurology 2011; 77: 18–25.

Lee MJ, Seo SW, Na DL, Kim C, Park JH, Kim GH, et al. Synergistic effects of ischemia and beta-amyloid burden on cognitive decline in patients with subcortical vascular mild cognitive impairment. JAMA Psychiatry 2014; 71: 412–22.

Love S, Miners JS. Cerebrovascular disease in ageing and Alzheimer's disease. Acta Neuropathol 2015; 131: 645–58.

Maclullich AM, Wardlaw JM, Ferguson KJ, Starr JM, Seckl JR, Deary IJ. Enlarged perivascular spaces are associated with cognitive function in healthy elderly men. J Neurol Neurosurg Psychiatry 2004; 75: 1519–23.

Martinez-Ramirez S, Pontes-Neto OM, Dumas AP, Auriel E, Halpin A, Quimby M, et al. Topography of dilated perivascular spaces in subjects from a memory clinic cohort. Neurology 2013; 80: 1551–6.

McKhann G, Drachman D, Folstein M, Katzman R, Price D, Stadlan EM. Clinical diagnosis of Alzheimer's disease: report of the NINCDS-ADRDA Work Group under the auspices of Department of Health and Human Services Task Force on Alzheimer's disease. Neurology 1984; 34: 939–44.

Pantoni L. Cerebral small vessel disease: from pathogenesis and clinical characteristics to therapeutic challenges. Lancet Neurol 2010; 9: 689–701.

Ramirez J, Berezuk C, McNeely AA, Scott CJ, Gao F, Black SE. Visible Virchow-Robin spaces on magnetic resonance imaging of Alzheimer's disease patients and normal elderly from the Sunnybrook Dementia Study. J Alzheimers Dis 2015; 43: 415–24.

Reijmer YD, van Veluw SJ, Greenberg SM. Ischemic brain injury in cerebral amyloid angiopathy. J Cereb Blood Flow Metab 2015; 36: 40–54.

Roher AE, Kuo YM, Esh C, Knebel C, Weiss N, Kalback W, et al. Cortical and leptomeningeal cerebrovascular amyloid and white matter pathology in Alzheimer's disease. Mol Med 2003; 9: 112–22.

Sachdev P, Wen W, Shnier R, Brodaty H. Cerebral blood volume in T2-weighted white matter hyperintensities using exogenous contrast based perfusion MRI. J Neuropsychiatry Clin Neurosci 2004; 16: 83–92.

Samarasekera N, Smith C, Al-Shahi Salman R. The association between cerebral amyloid angiopathy and intracerebral haemorrhage: systematic review and meta-analysis. J Neurol Neurosurg Psychiatry 2012; 83: 275–81.

Seo SW, Cho SS, Park A, Chin J, Na DL. Subcortical vascular versus amnestic mild cognitive impairment: comparison of cerebral glucose metabolism. J Neuroimaging 2009; 19: 213–19.

Thrane AS, Rangroo Thrane V, Nedergaard M. Drowning stars: reassessing the role of astrocytes in brain edema. Trends Neurosci 2014; 37: 620–8.

van Veluw SJ, Biessels GJ, Bouvy WH, Spliet WG, Zwanenburg JJ, Luijten PR, et al. Cerebral amyloid angiopathy severity is linked to dilation of juxtacortical perivascular spaces. J Cereb Blood Flow Metab 2016; 36: 576–80.

Verbeek MM, Kremer BP, Rikkert MO, Van Domburg PH, Skehan ME, Greenberg SM. Cerebrospinal fluid amyloid beta(40) is decreased in cerebral amyloid angiopathy. Ann Neurol 2009; 66: 245–9.

Wardlaw JM, Smith C, Dichgans M. Mechanisms of sporadic cerebral small vessel disease: insights from neuroimaging. Lancet Neurol 2013a; 12: 483–97.

Wardlaw JM, Smith EE, Biessels GJ, Cordonnier C, Fazekas F, Frayne R, et al. Neuroimaging standards for research into small vessel disease and its contribution to ageing and neurodegeneration. Lancet Neurol 2013b; 12: 822–38.

Weller RO, Hawkes CA, Kalaria RN, Werring DJ, Carare RO. White matter changes in dementia: role of impaired drainage of interstitial fluid. Brain Pathol 2015; 25: 63–78.

Weller RO, Preston SD, Subash M, Carare RO. Cerebral amyloid angiopathy in the aetiology and immunotherapy of Alzheimer disease. Alzheimers Res Ther 2009; 1: 6.

Williams S, Chalmers K, Wilcock GK, Love S. Relationship of neurofibrillary pathology to cerebral amyloid angiopathy in Alzheimer's disease. Neuropathol Appl Neurobiol 2005; 31: 414–21.

Yakushiji Y, Charidimou A, Hara M, Noguchi T, Nishihara M, Eriguchi M, et al. Topography and associations of perivascular spaces in healthy adults: the Kashima scan study. Neurology 2014; 83: 2116–23.